Collateral Sprouting of Peripheral Sensory Neurons Exhibits a Unique Transcriptomic Profile

Article *in* Molecular Neurobiology · July 2020

DOI: 10.1007/s12035-020-01986-3

Molecular Neurobiology
https://doi.org/10.1007/s12035-020-01986-3

Collateral Sprouting of Peripheral Sensory Neurons Exhibits a Unique Transcriptomic Profile

Dominique Lemaitre[1] · Maica Llavero Hurtado[2] · Cristian De Gregorio[3] · Maritza Oñate[4] · Gabriela Martínez[5,6,7] · Alejandra Catenaccio[8] · Thomas M. Wishart[2] · Felipe A. Court[7,8,9]

Received: 18 March 2020 / Accepted: 8 June 2020

Abstract

Peripheral nerve injuries result in motor and sensory dysfunction which can be recovered by compensatory or regenerative processes. In situations where axonal regeneration of injured neurons is hampered, compensation by collateral sprouting from uninjured neurons contributes to target reinnervation and functional recovery. Interestingly, this process of collateral sprouting from uninjured neurons has been associated with the activation of growth-associated programs triggered by Wallerian degeneration. Nevertheless, the molecular alterations at the transcriptomic level associated with these compensatory growth mechanisms remain to be fully elucidated. We generated a surgical model of partial sciatic nerve injury in mice to mechanistically study degeneration-induced collateral sprouting from spared fibers in the peripheral nervous system. Using next-generation sequencing and Ingenuity Pathway Analysis, we described the sprouting-associated transcriptome of uninjured sensory neurons and compare it with the activated by regenerating neurons. In vitro approaches were used to functionally assess sprouting gene candidates in the mechanisms of axonal growth. Using a novel animal model, we provide the first description of the sprouting transcriptome observed in uninjured sensory neurons after nerve injury. This collateral sprouting-associated transcriptome differs from that seen in regenerating neurons, suggesting a molecular program distinct from axonal growth. We further demonstrate that genetic upregulation of novel sprouting-associated genes activates a specific growth program in vitro, leading to increased neuronal branching. These results contribute to our understanding of the molecular mechanisms associated with collateral sprouting in vivo. The data provided here will therefore be instrumental in developing therapeutic strategies aimed at promoting functional recovery after injury to the nervous system.

Keywords Axonal regeneration · Collateral sprouting · Nerve injury · Sciatic nerve · Transcriptome

Electronic supplementary material The online version of this article (https://doi.org/10.1007/s12035-020-01986-3) contains supplementary material, which is available to authorized users.

✉ Felipe A. Court
felipe.court@umayor.cl

Dominique Lemaitre
dominiquelemaitre@udd.cl

Maica Llavero Hurtado
maica.llavero@roslin.ed.ac.uk

Cristian De Gregorio
crdegregorio@udd.cl

Maritza Oñate
maritza.onate@einsteinmed.org

Gabriela Martínez
gabriela.martinezb@gmail.com

Alejandra Catenaccio
alecatenaccio@gmail.com

Thomas M. Wishart
t.m.Wishart@ed.ac.uk

[1] Facultad de Medicina, Centro de Fisiología Celular e Integrativa, Universidad del Desarrollo, Santiago, Chile

[2] The Roslin Institute, University of Edinburgh, Edinburgh, UK

[3] Centro de Medicina Regenerativa, Facultad de Medicina Clínica Alemana, Universidad del Desarrollo, Santiago, Chile

[4] Department of Physiology, Faculty of Biological Sciences, Pontificia Universidad Católica de Chile, Santiago, Chile

[5] Biomedical Neuroscience Institute (BNI), Faculty of Medicine, University of Chile, Santiago, Chile

[6] Program of Cellular and Molecular Biology, Institute of Biomedical Sciences, Departamento de Neurología y Neurocirugía, Hospital Clínico, University of Chile, Santiago, Chile

[7] FONDAP Center for Geroscience (GERO) Brain Health and Metabolism, Santiago, Chile

[8] Center for Integrative Biology, Faculty of Sciences, Universidad Mayor, Santiago, Chile

[9] Buck Institute for Research on Aging, Novato, CA 94945, USA

Published online: 21 July 2020

Background

Peripheral nerve injuries lead to the loss of motor and sensory function, which can be recovered by the regeneration of axonal tracts [1, 2]. However, functional recovery after extended nerve damage is only partially achieved by regenerative mechanisms of the injured neuron [1, 3]. After diverse types of injury, compensatory circuits generated by collateral sprouting from intact axons can lead to target reinnervation, contributing to the recovery of motor and sensory functions [4–8]. In the clinics, anastomosis of the distal stump of an injured nerve to the lateral side of an intact donor nerve, a technique known as end-to-side neurorrhaphy, leads to functional recovery of the denervated target by the extension of collaterals from the intact nerve to the injured one [9, 10]. Currently, most studies aimed at promoting functional recovery after nerve injury have been focused on the mechanisms associated with axonal regeneration. However, despite its contribution to nervous system repair, little attention has been dedicated to elucidating the molecular mechanisms associated with collateral sprouting.

After a peripheral axonal injury, a shift in the gene expression pattern of damaged neurons increases their intrinsic neuronal growth capacity through expression of regeneration-associated genes (RAGs) [11, 12]. This transcriptomic change is partially induced by neuronal intrinsic signals generated in the injured region, which travel retrogradely to the soma activating a regrowth genetic program [13, 14]. In the case of intact neurons, collateral sprouting is triggered by extrinsic signals from injured fibers in the process of Wallerian degeneration [6, 15, 16]. In the peripheral nervous system (PNS), this degenerative program triggered by mechanical and toxic stimuli involves tissue changes characterized by axonal degeneration, differentiation of Schwann cells into a repair phenotype, myelin disintegration, macrophage invasion, and the secretion of neurotrophic factors, creating a permissive environment for axonal growth [17, 18]. We have demonstrated that after spinal cord hemisection, collateral sprouting from intact corticospinal tracts is greatly reduced in transgenic mice with delayed Wallerian degeneration (Wld^S) [6], revealing a role for this degeneration program in triggering collateral sprouting.

To date, transcriptional changes associated with collateral sprouting and sprouting-associated genes (SAGs) have been exclusively studied in the central nervous system (CNS). Sprouting of peri-infarct cortical neurons after stroke has been associated with the activation of an exclusive transcriptional profile, different from those activated by sprouting neurons during development [19, 20]. After spinal cord injury (SCI), the observed spontaneous functional recovery mediated by collateral sprouting of intact spinal tracts depends on the triggering of a unique sprouting transcriptome [21, 22], suggesting that the "degenerated" environment is able to induce transcriptomic changes and increase the intrinsic growth capacity of uninjured neurons. It is known that after a CNS injury, adult neurons do not efficiently regenerate due to the presence of an inhibitory environment and a diminished intrinsic growth capacity of adult neurons compared with development [23, 24]. Conversely, the greater intrinsic growth ability of adult peripheral neurons allows them to spontaneously regenerate after injury by activating a regeneration-associated genetic program [12]. This disparity became evident in dorsal root ganglia (DRG) injury models, in which central axons that project to the spinal cord fail to regenerate, while peripheral projections vigorously regrow after damage. It was demonstrated that a prior peripheral injury not only increases the axon outgrowth ability of peripheral branches but is also able to induce regeneration of central projections by regulation of growth-associated genes [23, 25]. The intrinsic difference between CNS and PNS neuronal growth capacity reveals the necessity of studying growth-associated mechanisms separately in both regions. This is crucial in order to effectively translate potential therapeutic strategies to promote functional recovery after a nervous system injury.

Here, by generating a model of partial sciatic nerve injury to mechanistically study collateral sprouting in the PNS, we found that neurons exposed to a Wallerian degeneration environment increase their intrinsic growth capacity in association with the activation of a unique transcriptome, which is different from the activated by regenerating injured neurons. Moreover, genetic manipulation of SAGs increases the branching capacity of adult DRG neurons in a stronger fashion than RAGs, suggesting that collateral sprouting is commanded by unique axonal growth mechanisms that potentiate not only axonal elongation but also axonal ramification, recapitulating morphological changes observed in developing neurons. Identification of novel growth-associated molecules here therefore expands the list of potential targets to investigate for ability to improve the functional outcome after severe nerve injuries.

Methods

Experimental Design To characterize the in vivo model of collateral sprouting in the PNS, animals were assigned to two groups: sham surgery (control) and L3 spinal nerve (SN) injury. Additionally, to confirm the presence of collateral sprouting of spared axons, two extra groups were formed: (1) a group that received a double injury, first an L3 spinal nerve injury, inducing collateral sprouting of L4 SN axons, and then, an L4 SN injury to induce degeneration of collateral sprouts and (2) another group that received, in addition to an L3 SN injury, an injection of an anterograde tracer to localize collateral sprouts. The sample size used for characterization analysis were 3 animals per group.

For in vitro and molecular analysis, animals were distributed in three experimental groups: sham surgery (control), L3 SN injury (ColSpr group), and sciatic nerve crush (AxReg group). The AxReg group was used as a documented model used to study the mechanisms of axonal regeneration. Comparisons were made between each group with control and also between ColSpr and AxReg groups, to stablish differences between both mechanisms, collateral sprouting and axonal regeneration. For in vitro analysis, three independent cultures were included.

Animals and Surgical Procedures Adult (8–12 weeks old) C57BL/6J female mice were obtained from the P. Catholic University and housed in the animal facility for all the experiments. Experimental procedures followed protocols approved by the Institutional Animal Care and Use Committees of the same Institution. For each surgery, animals were deeply anesthetized with a single dose of 2-2-2 tribromoethanol (330 mg/kg i.p.) (Sigma-Aldrich, cat no. T48402) and treated with tramadol (30 mg/kg i.p.) for 3 days post-surgery as analgesic. Post-operative care included monitoring of physical appearance and unprovoked behavior to determine the presence of pain. Animals with signs of autotomy were immediately excluded from the study and euthanized with a triple dose of 2-2-2 tribromoethanol (330 mg/kg i.p). Prior to surgeries, animals were shaved and sterilized in the surgical area and placed in ventral decubitus.

To injure the L3 SN, a skin incision was made in the midline of the lower back, at the level of L2-L5 lumbar vertebrae and muscles were separated. L2-L3 articular processes were removed and L3 DRG was exposed. At that moment, the mice were changed into a left lateral decubitus position to have a better view of the DRG. After removing the L3 transverse process, the L3 SN was exposed and transected using a micro-scissor (Lawton, cat no. 63-1403). Additionally, a 2-mm segment of the L3 SN was removed to avoid the possibility of axonal regeneration. In sham-operated mice, the L3 SN was exposed but left intact. Muscles were sutured with a 4–0 silk suture (Dafilon ®, Braun, cat no. C0936235) and the skin incision using metal suture clips (Fine Science Tools Inc., cat no. 12040-01). During recovery, mice were placed in a temperature-controlled chamber and allowed to survive for 7, 14, 21, and 40 days post injury (dpi). In the double-injury group, an L3 SN transection was made exactly as described above and 14 days later, animals were anesthetized and the previous surgical wound was reopened. L3-L4 articular processes were removed and the L4 DRG exposed. At that moment, mice were changed into a left lateral decubitus position to have a better view of the DRG. The distal stump of the previously injured L3 SN was exposed and 1–1.5-mm segment was carefully removed and saved for collateral sprouting analysis at 14 dpi. Then, the L4 SN was exposed and transected using a micro-scissor. A 1.5–2-mm segment of the L4 SN was removed to avoid axonal regeneration. For anterograde tracing of collateral sprouting, the L4 DRG was exposed following the same procedures described above, and using a 5-μl Hamilton syringe (Hamilton, cat no. 7634-01) with a 34G needle and a microinjection system (InjectoMate, Neurostar), 1 μl of biotinylated dextran amine (BDA) 10.000 MW tracer (Thermo Fisher, cat no. D1956) was injected directly into the L4 DRG in a 3-min period. Then, the L3 SN transection was performed as previously described. Animals of this group were allowed to survive for 14 dpi. For in vitro and molecular analysis, animals of the ColSpr group received an L3 SN transection and in the AxReg group a complete sciatic nerve crush was made. The control group consisted in a sham-operated mice. After surgeries, mice were allowed to survive for 3 or 7 dpi. For the sciatic nerve crush, a skin incision and muscle dissection were performed at the level of the sciatic notch to expose the right sciatic nerve. Using a Dumont no. 5 forceps (Fine Science Tools Inc. cat no. 11254-20), the sciatic nerve was three times crushed for 5 seconds (s). The skin was suture with metal clips.

Immunofluorescence Analysis After euthanizing the animals by terminal anesthetization, sciatic nerves of L3 SN-injured and sham-operated animals were dissected and 2–3-mm segments of L3 SN distal to injury (L3sn), L4 SN (L4sn), and sciatic nerve (Scn) proximal to the sciatic notch were removed for immunofluorescence and electron microscopy (EM) analysis. L4 DRG of the same animals and of the sciatic nerve-crushed group were removed for histological analysis. For immunofluorescence, tissue was fixed in 4% paraformaldehyde for 1 h, dehydrated with grade sucrose solution, and embedded and fast frozen in optimal cutting temperature compound (OCT Sakura Finetek). Ten-micrometers of transverse sections of nerve segments were obtained using a cryostat (Leica). Each DRG was entirely sectioned and serially mounted in four different slides to have the DRG structure fully represented. Sections were mounted on Superfrost Plus Slides (Thermo Fisher Scientific). For staining, slides were treated with a blocking-permeabilization solution (0.1% Triton X-100, 2% fish skin gelatin) for 1 h, immunolabeled with primary antibodies overnight and incubated with secondary antibodies in the same blocking solution for 2 h. Slides were mounted with Fluoromount (Sigma-Aldrich) and DAPI (Thermo Fisher cat no. D1306) for nuclear staining. The following antibodies were used: chicken anti-neurofilament medium chain (NFM), 1:2000 (EMD Millipore cat no. AB5735); rabbit anti-activating transcription factor 3 (ATF3), 1:500 (Santa Cruz cat no. sc-188); rabbit anti-neurofilament heavy chain (NFH), 1:1000 (Sigma-Aldrich cat no. N4142); rabbit anti-myelin basic protein (MBP), 1:500 (Sigma-Aldrich cat no. M3821); rabbit anti-p75 neurotrophin receptor (p75NTR), 1:500 (EMD Millipore cat no. 07-476), rat anti-CD11b, 1:500 (AbD Serotec cat no. MCA74G), anti-rat

Alexa-488, 1:1000 (Thermo Fisher cat no. A-21208); anti-chicken Alexa-594, 1:1000 (Thermo Fisher cat no. A-11042); anti-rabbit Alexa-488, 1:1000 (Thermo Fisher cat no. A-11034); anti-rabbit Alexa 546, 1:1000 (Thermo Fisher cat no. A-11035); Alexa-488-conjugated Avidine, 1:500 (Thermo Fisher cat no. A-21370). Images were captured with an inverted fluorescence microscope (Olympus IX71) equipped with a × 10 and × 40 objectives and fitted with a QICAM Fast 1394 camera (Qimaging). Quantification of the nerve area covered by NFM, CD11b, and p75NTR staining was made separately in the intact and injured area guided by myelin or axonal staining. For collateral sprouting quantification, the density of NFM-positive particles was obtained from three images of the L3 SN region of each animal. Triple-positive ATF3/NFM/DAPI neurons were quantified in six serial sections of each L4 DRG. Image processing was made using the ImageJ software.

Electron Microscopy For EM analysis, nerve segments were fixed overnight in EM fixative solution (2.5% glutaraldehyde, 0.01% picric acid and 0.1 M cacodylate buffer, pH 7.4). After incubation in the same buffer, tissues were immersed in 1% OsO_4 for 1 h, followed by 2 h incubation with 2% uranyl acetate and dehydrated with graded ethanol solutions. Tissues were included in epoxy resin, cured at 60 °C overnight, and added to pre-crafted epoxy resin blocks. One-micron thick semi-thin sections were obtained and stained with 1% toluidine blue for light microscopy. Ultra-thin 70-nm sections were obtained using an ultra-microtome, mounted in copper grids and contrasted with 1% uranyl acetate and lead citrate. Grids were examined with a transmission electron microscope (FEI, Tecnai 12) operated at 80 kV and semi-thin sections with a light microscope (Nikon, Eclipse E200). Image processing was made using the ImageJ software. Myelinated axons density was quantified in semi-thin sections of L3sn region and myelin g-ratio (axon diameter/myelin diameter) was measured in 40 axons per time point from EM images.

DRG Culture after Conditioning Lesions The intrinsic growth capacity of L4 DRG neurons was analyzed in vitro 7 days after receiving an L3 SN transection (ColSpr group), a sciatic nerve crush (AxReg group), or sham operation (control group). To this end, animals were euthanized by terminal anesthetization and the right L4 DRG was removed. For preparation of dissociated DRG neurons, dissected L4 DRG were immediately transferred to pre-chilled DMEM/F12 medium (Thermo Fisher, cat no. 12500062) and then digested with 3% type I collagenase (Thermo Fisher, cat no. 7100017) in DMEM/F12 during 1.5 h at 37 °C. Later, the DRG were digested with 2.5% trypsin (Thermo Fisher, cat no. 5090046) in Hank's balanced salt solution without calcium/magnesium during 25 min at 37 °C. A posterior mechanical dissociation was made with a fire-polished Pasteur pipette. Cells were centrifuged at 700*g* for 5 min, seeded in poly-L-lysine and laminin pre-treated covers glasses in DMEM/F12 supplemented with 10% fetal bovine serum (Thermo Fisher, cat no. 10437-028), 2% B27 (Thermo Fisher, cat no. 17504044), and 10 μM cytosine arabinoside (Sigma-Aldrich, cat no. C6645), and then, incubated at 37 °C with 5% CO_2 for 24 and 48 h. Neurite outgrowth was quantified by Sholl analysis as previously described (Ferreira et al. 2014), using 30 isolated sensory neurons of each culture (three independent cultures for each group). Concentric circles of 10-μm radius were overlapped on neurons masks around the soma until 1000 μm of distance and the maximum radius reached by neurites was determined as a measure of neurite length. Neurite branching was quantified as the number of intersections of neurites with the concentric circles.

RNA Extraction and Quantitative Real-Time Polymerase Chain Reaction For molecular analysis, ribonucleic acid (RNA) was isolated from a pool of six L4 DRG from different animals, obtaining three independent pools per group. Total messenger RNA (mRNA) was purified using the RNeasy Mini Kit (Qiagen, cat no. 74104) and complementary deoxyribonucleic acid (cDNA) was synthesized from 0.5 μg of RNA with the High-Capacity cDNA Reverse Transcription Kit (Thermo Fisher, cat no. 4368813). Purified RNA was used for RNA sequencing (described below) and RNA extraction and quantitative real-time polymerase chain reaction (qRT-PCR). Quantitative real-time PCR was carried out using SYBR Green assay (Kapa biosystem, cat no. KK4601) and Mx3005P qPCR System (Stratagene). Samples were run in duplicates. mRNA expression was normalized to actin expression. Transcript levels were quantified by using the ΔΔCt value method. The list of primers used for analysis of neuronal injury and validation of transcriptomes are shown in Table 1.

RNA Sequencing and Bioinformatics RNA sequencing (RNA-seq) analysis was performed in the control, ColSpr, and AxReg groups at 3 dpi. RNA samples were sent to the Genomics and Bioinformatics Center of the Faculty of Sciences of Universidad Mayor for RNA-seq analysis. RNA quantification and quality control assays were performed with a 2100 Bioanalyzer system using the Agilent RNA 6000 Pico Kit (Agilent Technologies, cat no. 5067-1513). Then, standard mRNA-Seq libraries were constructed from poly-A selected mRNA using a TruSeq® Stranded mRNA kit (Illumina, cat no. RS-122-2101), with an RNA input of 500 ng. A quality control of the libraries was made with the 2100 Bioanalyzer system using an Agilent DNA 1000 kit (Agilent Technologies, cat no. 5067-1504), followed by a library quantification with the Step One Plus Real-Time PCR system (Thermo Fisher), using the Illumina Library Quantification kit, Universal qPCR Mix (Kapa Biosystems). Then, the

Table 1 Primers used for qPCR validation of transcriptomes

Gene symbol	Forward primer (5′ to 3′)	Reverse primer (5′ to 3′)
Atf3	GAGGATTTTGCTAACCTGACACC	TTGACGGTAACTGACTCCAGC
Serpine 1	TTCAGCCCTTGCTTGCCTC	ACACTTTTACTCCGAAGTCGGT
Vgf	AAGGATGACGGCGTACCAGA	TGCCTGCAACAGTACCGAG
Chrna6	TAAAGGCAGTACAGGCTGTGA	AAAATGCACCGTGACGGGAT
Caly	TGCATCCTCCGCATCTACAC	ATCCTGGTCTCCTGCTTCCT
Tceal6	GAGAAGCAGGGAAAGTCTGAC	TTCCGGGGCACATAATCTTCA
Gal	GGCAGCGTTATCCTGCTAGG	CTGTTCAGGGTCCAACCTCT
Sprr1a	GCCTGAAGACCTGATCACCA	GGTAGCACAAGGCAATGGGA
Cckbr	GATGGCTGCTACGTGCAACT	CGCACCACCCGCTTCTTAG
Fgf3	CCATCAAAGGGCTCTTTTCTGG	CGTTGTAGTGATCCGAAGCAT
Gdf10	CAGGACATGGTCGCTATCCAC	ACAGGCTTTTGGTCGATCATTTC
Acta2	GTCCCAGACATCAGGGAGTAA	TCGGATACTTCAGCGTCAGGA
Arhgef5	CGCACTGAGACTCAAAGTGAA	GGAGGCACTGAACTTGTGG
Mdfi	CCACGACCACCTCTCAGAAC	GACAGGACAGTATGCAGTGGA
Ctgf	GGGCCTCTTCTGCGATTTC	ATCCAGGCAAGTGCATTGGTA

libraries were sent to BGI Tech Solutions Co. (Hong Kong, China) for RNA-seq, which was performed using the HiSeq 2000 sequencing platform (Illumina) with 100-bp paired-end parameters. Quality control and verification of sequence number and adaptor absence was performed with Fast QC (Quality Control Tool for High Throughput Sequence Data). A contamination control was also made with Beta Onecodex platform.

DRG Electroporation DRG neuron co-electroporation was performed using the NEPA21 electroporator (Nepagene, Japan) according to the manufacturer's recommendations. Briefly, 1×10^5 DRG dissociated neurons (as described above) from adult mice were resuspended in Opti-MEM medium with a mixture of 5 μg of pCSCMV:tdTomato plasmid (Addgene, cat no. 30530) and 5 μg of the following genes plasmids tagged with green fluorescent protein (GFP): Atf3 (Origene, cat no. MR201634), fibroblast growth factor 3 (Fgf3) (Origene, cat no. MR222923), growth differentiation factor 10 (Gdf10) (Origene, cat no. MR207626), actin alpha 2 (Acta2) (Origene, cat no. MR205873), rho guanine nucleotide exchange factor 5 (Arhgef5) (Origene, cat no. MR215297), and GFP alone. This mixture was electropored with a poring pulse (two pulses of 150 V with 5-ms pulse length, with 50 ms of interval between the pulses, 10% decay, rate with + polarity) followed by a transfer pulse (five pulses of 20 V with 50-ms pulse length, with 50 ms of interval between pulses, 40% decay, rate with ± polarity). After the electroporation, cells were immediately cultured in poly-L-lysine and laminin pretreated covers glasses in DMEM/F12 supplemented with 10% fetal bovine serum (FBS), 2% B27, and 10 μM cytosine arabinoside and incubated at 37 °C with 5% CO_2 for 48 h. Neurons' growth capacity was quantified by Sholl analysis as described above.

Statistical Analyses For histological characterization of the model by immunofluorescence and EM, a sample of $n = 3$ mice per group was used. Immunofluorescence and EM analysis values were obtained from the average of the measure of three or six images per animal in each group. For g-ratio analysis, 40 axons per control and time point were measured. Histological data was analyzed using one-way ANOVA test, followed by Tukey post hoc test for multiple comparisons between groups. Evaluation of the intrinsic growth capacity of L4 DRG neurons per group (Control, ColSpr, and AxReg) was made in vitro. For Sholl analysis, 30–35 neurons were measured in each culture per group and three independent cultures were analyzed in total. Assessment of the intrinsic growth capacity of L4 DRG neurons after gene overexpression by Sholl analysis included the measure of 10 electroporated neurons per group in each culture, and three independent cultures were analyzed in total. Statistical significance in Sholl analysis was made using two-way ANOVA followed by Bonferroni post hoc tests. Comparisons of the neurite length of L4 DRG neurons after gene overexpression was made between groups and between each group with the control column. Statistical analysis of neurites length was determine using one-way ANOVA test, followed by Tukey post hoc test for multiple comparisons between groups or by Bonferroni test for multiple comparisons between each group with control column. Analyses were considered statistically significant with a $p < 0.05$.

For RNA-seq data, differential expression analyses were made with Cuffdiff tool (Cufflinks software) and differentially expressed genes were selected based on q-value < 0.05 (p value corrected by a false discovery rate (FDR) of 5%). Only transcripts that passed the less stringent test were considered in the analysis. We used t test between the triplicates

of each group, two-tailed distribution, and two-sample unequal variance (heteroscedastic).

For Ingenuity Pathway Analysis (IPA), transcripts that passed the statistical filters stated above were analyzed using IPA application (Ingenuity Systems). IPA was used to obtain further insight into potential cellular pathways underlying AxReg and ColSpr. IPA was utilized as previously described [26, 27]. Canonical pathway function was used for the identification of known pathways within these datasets. IPA contains a library of biological pathways published in the literature that are ranked by significance of the association between the dataset and the canonical pathway. The significance is defined by (1) the ratio of the number of proteins from the dataset that map on the pathway divided by the total number of genes within the canonical pathway, and (2) a p value calculated using Fisher's exact test that determines if the probability of association between the proteins in the dataset and in the pathway is due to chance. Secondly, to further understand the molecular pathways underlying ColSpr, only the transcripts exclusively regulated in ColSpr in relation to AxReg were analyzed using the Network function in IPA.

Results

Wallerian Degeneration in the Sciatic Nerve After L3 Spinal Nerve Injury

To study the molecular mechanisms of collateral sprouting in the PNS, we generated a model of partial sciatic nerve injury. In mice, the sciatic nerve is mainly constituted by anastomosis of the L3 and L4 spinal nerves (SN), with a low contribution from L5 [28]. To partially damage the sciatic nerve, we transected L3 SN to induce Wallerian degeneration in this subset of axons and leave spinal nerves L4 and L5 uninjured (Fig. 1a, Supplementary Fig. 1A). In this manner, direct contact between intact axons and the axonal "degenerated" environment is achieved in the sciatic nerve trunk. In addition, somas of sensory neurons projecting to L3, L4, or L5 spinal nerves can be isolated from respective DRG for downstream analysis.

We first characterized Wallerian degeneration of spinal and sciatic nerves 7 days after L3 SN injury, when Wallerian degeneration is significantly advanced [29, 30]. Using toluidine-stained semi-thin sections examined by light microscopy and immunofluorescence staining, we analyzed the nerve structure of L3 and L4 SN segments (L3sn and 4Lsn, respectively) and a segment of the sciatic nerve trunk formed by L3, L4, and L5 contribution (Scn). In a control uninjured nerve, condensed myelin structure is visualized in semi-thin sections (Fig. 1b). Immunostaining analysis for different cellular markers showed intact myelin and axonal density, with MBP and NFM, respectively, and a low presence of macrophages and repair-state Schwann cells, by CD11B and p75NTR staining, respectively (Fig. 1b, first row). The distal stump of L3 SN (L3sn) showed myelin disintegration and consequent loss of axonal structure in toluidine-stained semi-thin sections examined by light microscopy. In addition, immunofluorescence analysis revealed axonal staining loss, massive macrophage invasion, and differentiation of Schwann cells into a repair phenotype, common hallmarks of the Wallerian degeneration process (Fig. 1b, second row). In L4 SN (L4sn), myelin sheaths and axonal staining were comparable with uninjured control nerves, without signs of macrophage infiltration or Schwann cell differentiation (Fig. 1b, third row). At the level of the sciatic nerve trunk (Scn), two regions were clearly identified: an intact area, with a histological structure equivalent to control nerves in toluidine-stained sections and immunofluorescence images, and an injured area presenting the hallmarks of Wallerian degeneration, comparable with L3sn (Fig. 1b, fourth row). Quantitative analysis for the different markers showed significant differences between the two regions (Fig. 1c–f and Supplementary Fig. 1B).

To assess if sensory neurons projecting to the L4 SN were completely spared from damage, the expression of the neuronal injury marker ATF3 was examined in L4 DRG neurons after L3 SN injury (ColSpr) by immunofluorescence and RT-qPCR. Analysis of L4 DRG neurons after a sciatic nerve crush injury was used as a positive control (AxReg). Nuclear

Fig. 1 Characterization of Wallerian degeneration in sciatic nerve after L3 spinal nerve transection. **a** Schematic representation of the L3 spinal nerve injury model to study collateral sprouting. L3 spinal nerve (L3sn), L4 spinal nerve (L4sn), and the whole sciatic nerve trunk (Scn) are indicated. **b** Toluidine-stained semi-thin transverse sections (first column) and images immunostained against CD11b (red) and MBP (green) or NFM (red) and P75NTR (green). DAPI (blue) was used as a nuclear stain. Control corresponds to a sciatic nerve segment of sham-operated animals. Scale bars, 40 μm. The dotted line shows the frontier between intact and degenerated areas of the Scn. **c–e** Quantification of the area covered by NFM, CD11b, and P75NTR staining in intact and degenerated areas of whole sciatic nerve images of control and injured nerves. Intact and degenerated areas were defined based on MBP staining. **f** Transverse section of the whole sciatic nerve 7 days after L3sn injury, immunostained against NFM (red) and with DAPI (cyan) as nuclear marker. Scale bar, 100 μm. **g** Immunofluorescence images of L4 DRG of uninjured (control), sciatic nerve crushed (AxReg), and L3sn injured (ColSpr) animals at day 3 post-injury, stained against ATF3 (red) and NFM (green). DAPI (blue) was used as nuclear stain. Scale bar, 50 μm. **h** Quantification of the percentage of ATF3-positive neurons in L4 DRG in control, AxReg and ColSpr conditions at 3 dpi. **i** Quantification of ATF3 mRNA in L4 DRG in control, AxReg and ColSpr at 3 dpi. Data is shown as mean ± S.E.M. Comparisons for immunofluorescences were made between all columns ($n = 3$). Statistical significance was determined by one-way ANOVA followed by Tukey's post hoc test. For DRG immunofluorescence and mRNA levels analysis, comparisons were made between control and the other conditions ($n = 3$). Statistical significance was analyzed by one-way ANOVA followed by Bonferroni's post hoc test (*$p < 0.05$, ** $p < 0.01$, *** $p < 0.001$)

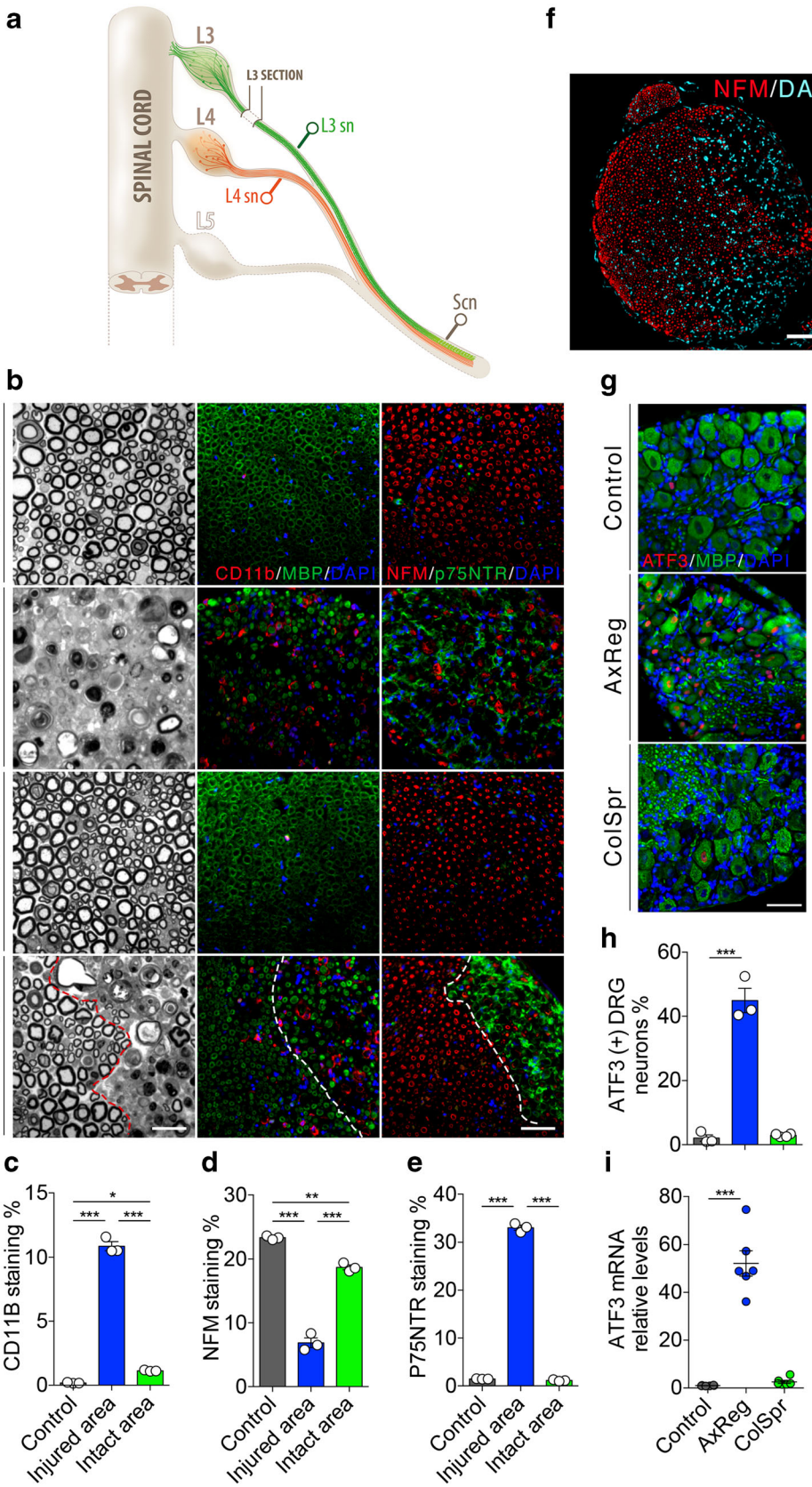
a
L3
L3 SECTION
L4
L3 sn
SPINAL CORD
L4 sn
L5
Scn
f
NFM/DAPI
b
Control
L3sn
L4sn
Scn
CD11b/MBP/DAPI
NFM/p75NTR/DAPI
g
Control
AxReg
ColSpr
ATF3/MBP/DAPI
h
ATF3 (+) DRG neurons %
c
CD11B staining %
d
NFM staining %
e
P75NTR staining %
i
ATF3 mRNA relative levels
Control
Injured area
Intact area
AxReg
ColSpr

staining and mRNA quantification in L4 DRG neurons after L3 SN injury remained at basal levels at 3 days post-injury (dpi) (Fig. 1g–i), as in control nerves, confirming that L4 spinal nerve axons were not injured after L3 spinal nerve injury.

Collaterals Are Produced by L4 Spinal Nerve Uninjured Neurons

To determine the presence of axon collaterals, we analyzed L3 SN distal to the nerve section, as in this region all axons are degenerated and this spinal nerve is continuous with undamaged axons projecting to the sciatic nerve from L4 SN. Since axon collaterals and regenerating fibers are indistinguishable, a 2mm segment of L3 SN was removed to completely prevent axonal regeneration (Fig. 2a). At 7 days post-injury, only few collaterals, visualized as neurofilament medium subunit (NFM)-positive puncta, were detected in the L3 SN distal stump (Fig. 2b). However, at 14 and 21 dpi, a significant increase in the density of NFM puncta was observed, suggesting the progressive invasion of collaterals to this nerve region (Fig. 2b, c). To verify that the NFM-positive particles observed were derived from uninjured L4 SN, a double-injury model was used, in which 14 days after L3 SN injury an L4 SN transection was performed to induce axonal degeneration along any extended collaterals (Fig. 2a). Compared to 14 dpi, 7 days after the second injury in L4 SN, the density of NFM-positive puncta in L3 SN sections was significantly reduced (Fig. 2b, c), ruling out the possibility that these puncta correspond to regenerating axons, and strongly suggesting they correspond to axon collaterals derived from uninjured axons.

To further confirm that collaterals in L3 SN were extended by uninjured L4 SN, sensory neurons of L4 DRG were anterogradely traced with BDA before L3 spinal nerve transection (Supplementary Fig. 1C). At 14 dpi, double-stained BDA/NFM-positive particles were observed by immunofluorescence in L4 SN sections, corresponding to axons of BDA-labeled L4 DRG neurons (Fig. 2d). As expected, several BDA/NFM-positive sprouts were found associated to degenerated areas of the L3 SN and sciatic nerve (Fig. 2d, bottom), confirming the presence of collaterals extended from L4 spinal nerve axons.

Collateral Sprouts Mature in Size and Become Myelinated

Our data demonstrate that after L3 SN transection, the distal stump of this spinal nerve becomes invaded by axon collaterals derived from uninjured axons projecting from the L4 SN branch. We therefore use this region to study the appearance and maturation of these axonal extensions. We observed scarce thinly myelinated axons in toluidine-stained sections and electron microscopy images at 14 dpi (Fig. 3a), suggesting collaterals become myelinated. This density contrasts with the high level of regenerated remyelinated fibers reported 14 days after a nerve crush injury [31, 32]. At 21 dpi, a mild increase in myelinated axonal collaterals was observed, with a greater significant increase at 40 dpi (Fig. 3a, b). The g-ratio of collateral sprouts, as a measure of the degree of myelination, at 21 days was higher than that in control nerve axons, while at 40 dpi lower values were calculated compared with control (Fig. 3c). Axonal size distribution after L3 SN injury showed progressive changes in time, suggesting collateral sprouts maturation (Fig. 3d).

Analysis of the Intrinsic Growth Capacity of Sensory Neurons Conditioned by Wallerian Degeneration

To determine if Wallerian degeneration of L3 SN is capable of increasing the intrinsic growth capacity of intact L4 SN neurons, we assessed neurite outgrowth of L4 DRG neurons in vitro by Sholl analysis 7 days after L3 SN transection (ColSpr). We compared this with the growth of L4 DRG neurons 7 days after receiving a direct sciatic nerve crush (AxReg). We used sham surgery as control (Control). After 24 and 48 h in culture, L4 DRG neurons of the AxReg condition showed a significant increase in the Sholl analysis parameters' maximum radius and number of intersections, as measures of neurite length and neurite branching, respectively, compared with control (Fig. 4a–e). This agrees with reported data describing an increase in elongation and number of growing neurites in sensory neurons after a conditioning lesion [33, 34]. After 24 h in culture, L4 DRG neurons of the ColSpr condition showed a significant increase in the maximum radius (Fig. 4a, b) and number of intersections (Fig. 4d), compared with control neurons. However, this increase in both parameters did not reach the levels observed in L4 DRG-injured neurons, being in an intermediate position between control and AxReg conditions. After 48 h in vitro, neurons conditioned by Wallerian degeneration reduced differences in neurite length compared to control neurons (Fig. 4c). Nevertheless, a significant increment in neurite branching was maintained (Fig. 4e), demonstrating different morphological changes in neurite growth in both groups.

Identification and Description of the Collateral Sprouting-Associated Transcriptome

To determine if the increase in the intrinsic growth capacity of intact sensory neurons triggered by the exposure to the degenerated environment is related to the activation of a specific growth transcriptional program, we performed RNA sequencing (RNA-seq) analysis of L4 DRG neurons after L3 spinal nerve transection (ColSpr). To define differences between the collateral sprouting and regeneration transcriptomes, we analyze L4 DRG neurons after a complete

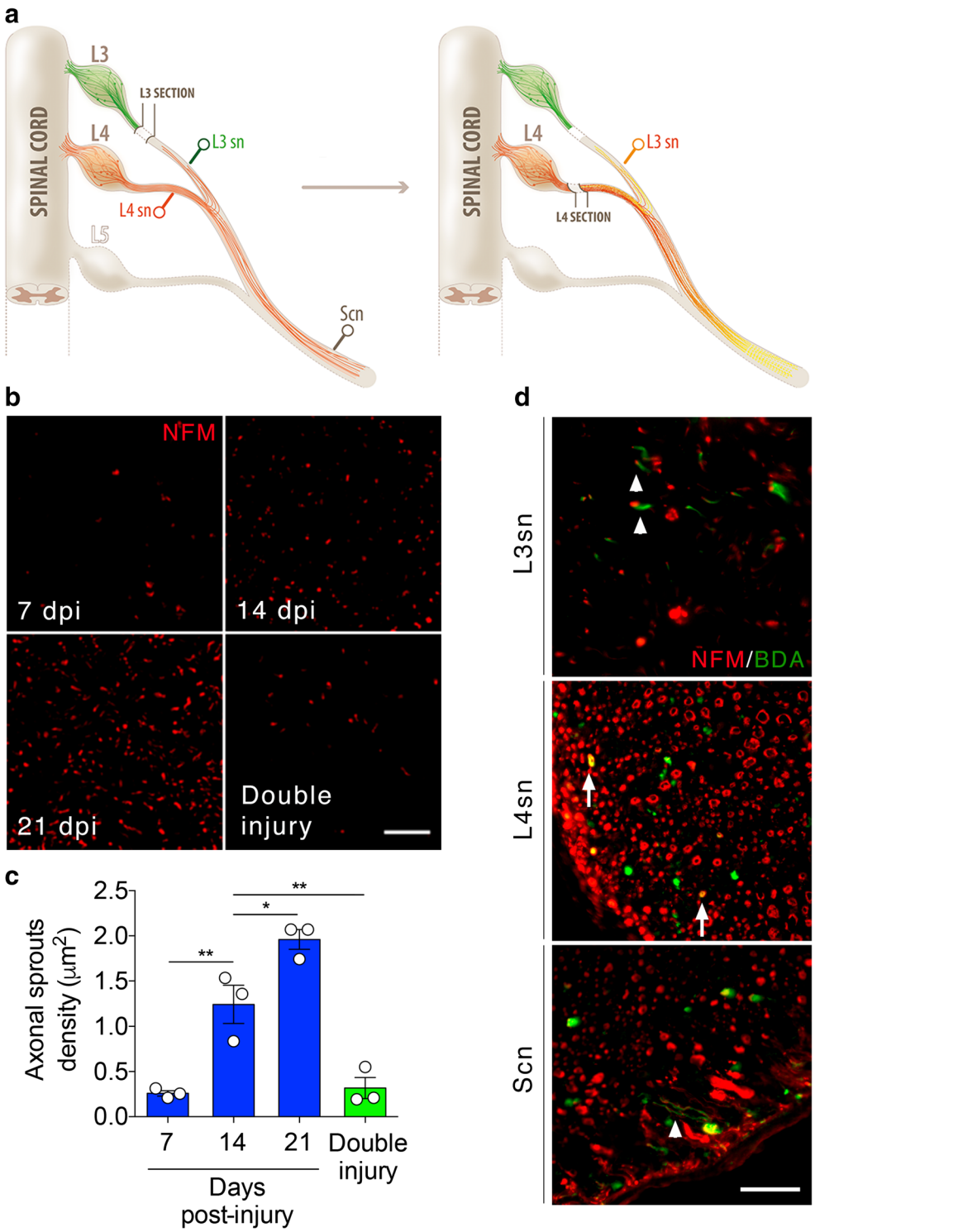

Fig. 2 L3 spinal nerve transection triggers axonal collaterals from intact L4 spinal nerve. **a** Schematic representation of the double-injury experiment. A first L3sn transection is performed and 14 days later, an L4sn transection is performed as indicated. Collateral sprouting was study in the L3sn segment. **b** Immunofluorescence images of L3sn transverse sections stained against NFM (red) at 7, 14, and 21 days post-L3sn injury (dpi) and 7 days after the double injury. Scale bar, 40 μm. **c** Quantification of the density of NFM-positive puncta in immunofluorescence images of L3sn transverse sections as shown in **b**. **d** Representative immunofluorescence images of L3sn, L4sn, and Scn, after anterograde tracing of L4sn collaterals. Immediately before L3sn transection, 1 μl of BDA tracer was injected in L4 DRG. Images correspond to transverse sections at 14 dpi showing colocalization of BDA (green) and NFM (red) staining. Arrows indicate BDA- and NFM-positive axons in intact L4sn and arrowheads show BDA- and NFM-positive collaterals in degenerated areas of L3sn and Scn segments. Scale bar, 40 μm. Data is shown as mean ± S.E.M. Comparisons were made between all columns with $n = 3$ animals per group and three images per animal were analyzed. Statistical significance was determined by one-way ANOVA followed by Tukey's post hoc test (for comparisons between 7 and 14 dpi, $^{**}p = 0.0034$; between 14 and 21 dpi, $^{*}p = 0.0212$; 14 dpi and after double injury $^{**}p = 0.005$)

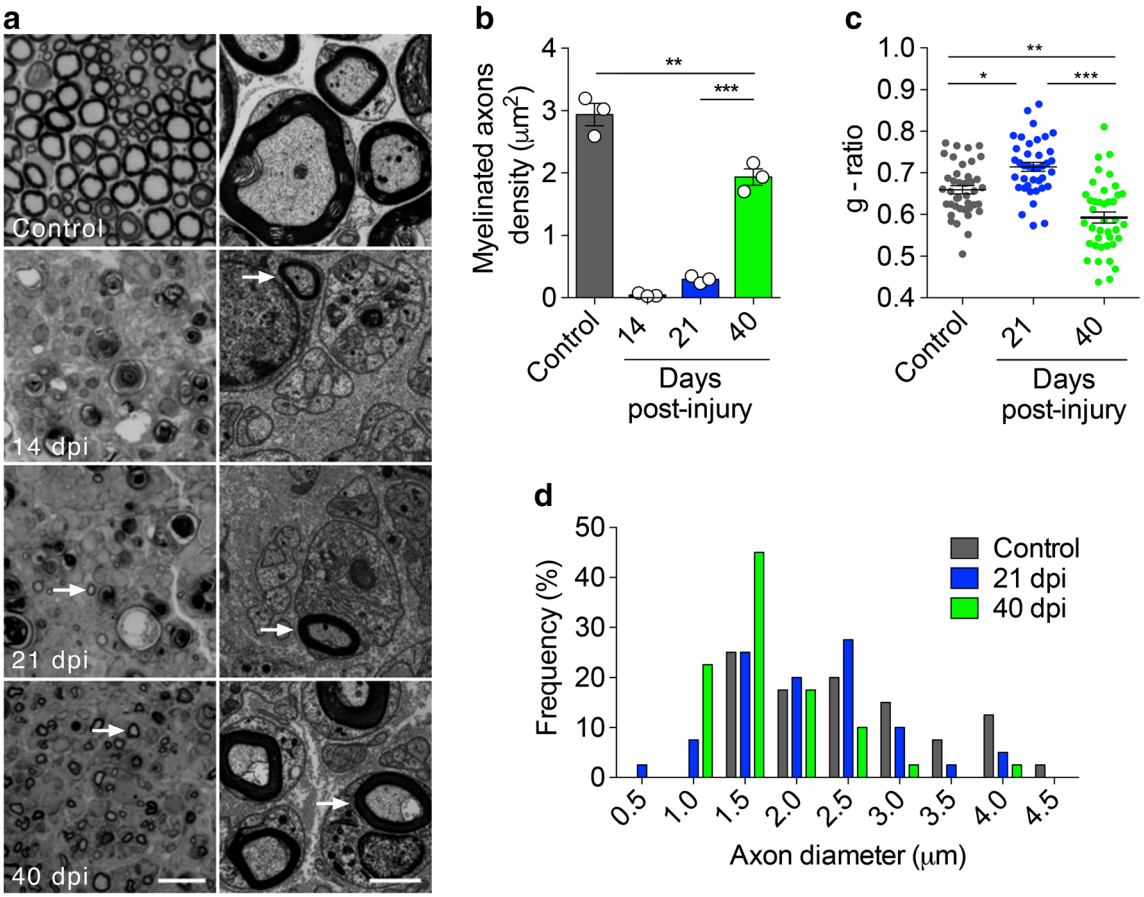

Fig. 3 Maturation and myelination of L4sn collaterals. **a** Toluidine blue–stained semi-thin sections (left) and electron microscopy (right) images of L3sn at 14, 21, and 40 days after L3sn injury. Control images correspond to nerves of sham-operated animals. Arrows indicate myelinated axons. Scale bar, 10 μm (left), 3 μm (right). **b** Quantification of myelinated axon density in L3sn Toluidine blue–stained semi-thin sections images at the indicated time points. **c** Scatter dot plot of myelinated axons g-ratio in control nerves and at 21 and 40 days after L3sn injury. **d** Frequency histogram of L3sn myelinated axon sizes obtained from EM images at different time points after L3sn injury and in control nerves. Data is shown as mean ± S.E.M. Comparisons were made between all columns with $n = 3$ animals per group and three images per animal were analyzed for myelinated axonal density analysis. For the frequency histogram and g-ratio analysis, 40 axons per time point were measured. Statistical significance was determined by one-way ANOVA followed by Tukey's post hoc test (in **b**, for comparisons between control and 40 dpi, $^{**}p = 0.0011$; between 21 and 40 dpi, $^{***}p < 0.0001$. In **c**, for comparisons between control and 21 dpi, $^{*}p = 0.0025$; between control and 40 dpi, $^{**}p = 0.0002$; between 21 and 40 dpi, $^{***}p < 0.0001$)

sciatic nerve crush injury (AxReg). Sham-operated animals were used as control condition. The analysis was carried out 3 days after lesions, a time at which the extension of collaterals has not yet started but the regeneration-associated genetic network is fully activated [14]. We found that L4 DRG neurons exposed to a degenerated environment (ColSpr) activated a transcriptome with 392 significantly differentially expressed transcripts, compared with control condition. Interestingly, 218 transcripts were exclusively regulated and 174 were shared with the AxReg transcriptome (Fig. 5a-c). The amount of significantly differentially expressed transcripts was substantially higher in AxReg (2884) than in ColSpr (392), compared with control (Additional files 1 and 2). Moreover, volcano plots showed that the magnitude of transcripts change was larger in AxReg than in ColSpr (Fig. 5a, b). Most of the shared transcripts were downregulated in both conditions, represented as red dots in volcano plots. However, exclusively regulated transcripts in ColSpr showed a clear tendency towards the upregulation (Fig. 5b, 181 upregulated, 33 downregulated), while in AxReg the proportion of up- and downregulated exclusive genes was more balanced (Fig. 5a, 1111 upregulated, 1032 downregulated).

When analyzed using software such as Ingenuity Pathway Analysis (IPA—a hand-curated interactome database produced from peer reviewed, published literature, used with stringent "experimentally observed only" filtering parameters), we found that predicted downstream consequences of these molecular perturbations were similar in terms of the majority of canonical cascades within both conditions. These include but are not limited to molecular processes known to govern actin cytoskeleton and acute phase response signaling cascades (Fig. 5d and Supplementary Fig. 2). Other growth-associated molecules

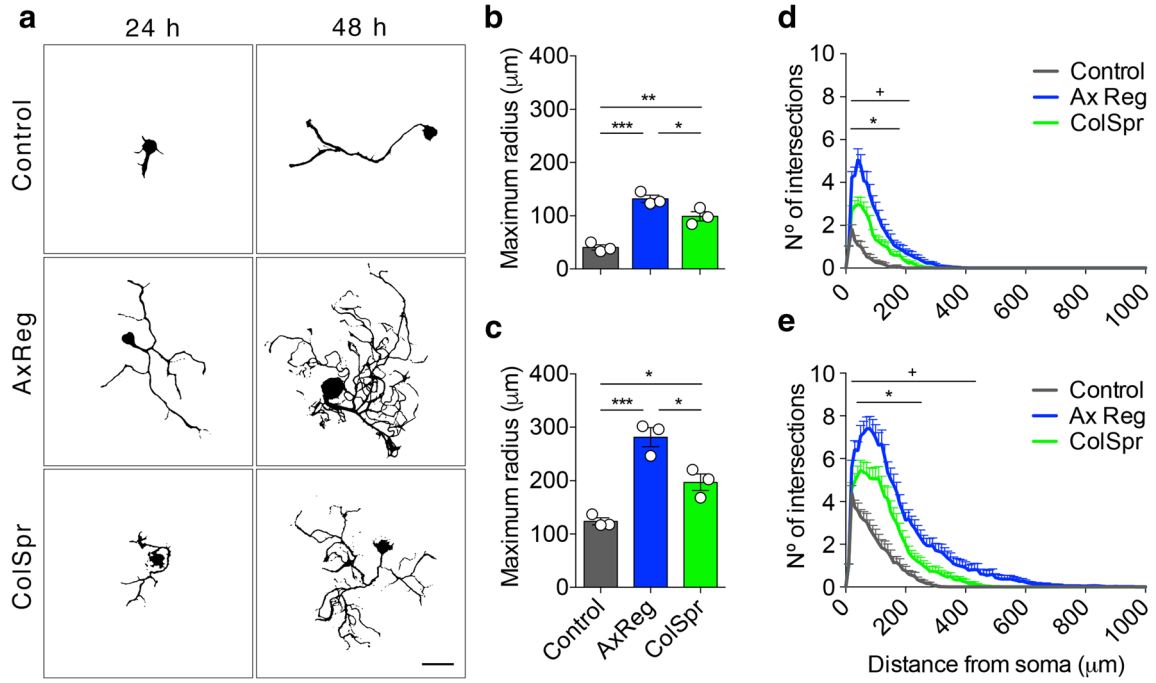

Fig. 4 The intrinsic growth capacity of L4 DRG neurons increase after Wallerian degeneration conditioning. L4 DRG neurons were removed 7 days after sham surgery (control), sciatic nerve crush (AxReg), or L3sn transection (ColSpr) and cultured for 24 and 48 h. (**a**) Representative immunofluorescent images of L4 DRG neurons after 24 and 48 h in vitro immunostained against MAP2. Scale bar, 50 μm. (**b**–**e**) Neurites outgrowth analysis of L4 DRG neurons. Concentric circles of 10-μm radius were overlapped on neuron masks around the soma until 1000 μm of distance. The maximum radius reached by neurites was determined in each condition after 24 h (**b**) and 48 h (**c**) in vitro. The intersections of neurites with concentric circles were quantified in each condition after 24 h (**d**) and 48 h (**e**) in vitro and plotted against the distance of concentric circles from the soma. Neurite outgrowth analyses were made in 30 neurons per condition in each culture and three independent cultures were analyzed ($n = 3$). Data is shown as mean ± S.E.M. For maximum radius, comparisons were made between all columns and statistical significance was determined by one-way ANOVA followed by Tukey's post hoc test (in **b**, for comparisons between control and AxReg, $***p = 0.0002$; between control and ColSp, $**p = 0.0027$, between AxReg and ColSpr, $*p = 0.0413$. In **c**, between control and AxReg, $***p = 0.0005$; between control and ColSpr, $*p = 0.0240$, between AxReg and ColSpr, $*p = 0.0126$). In **d**–**e**, comparisons were made between control and each condition and statistical significance was analyzed by two-way ANOVA followed by Bonferroni's post hoc test ($^{+}$comparisons between control and AxReg with $p < 0.05$ and *comparison between control and ColSpr with $p < 0.05$)

such as Cyclin D, Smad2/3, Ephrin-A, Ephrin-B, and Netrin were upregulated in ColSpr while down- or not regulated in AxReg. Smad2 and Smad3 signaling mediates axonal sprouting-promoting effects after CNS injury [20] and ephrins and netrins are implicated in axonal guidance and growth during neurodevelopment and after nerve injury [35–37].

The top ranked canonical pathways identified in independent analysis of ColSpr-induced transcriptional alterations include mechanistic classifications such as hepatic/hepatic stellate cell activation, GP6 signaling pathway, axonal guidance signaling, osteoarthritis pathway, and caveolar-mediated endocytosis signaling. While the nomenclature/subclassifications can seem confusing to those not familiar with IPA, it is important to note that the molecules comprising these subgroupings are frequently associated with cellular activation and growth programs. All of these pathways, except axonal guidance signaling, were significantly more regulated in ColSpr than AxReg, suggesting differential activation of genetic modules.

IPA of transcripts exclusively regulated in ColSpr showed the regulation of networks implicated in cell signaling and interaction, cell morphology, cell death/survival, connective tissue development and function, and skeletal and muscular system development. One of the highly activated networks involved upregulation of Smad3, Gdf10, Arhgef5, and Acta2 transcripts (Supplementary Fig. 3). Interestingly, Smad3 and Gdf10 have been implicated in cortical neuron plasticity after stroke [20].

Additional file 1 - Gene candidates of the axonal regeneration transcriptome (Additional file 1_AxReg Candidates.xlsx).

List of gene candidates obtained after t-test between triplicates of control and axonal regeneration (AxReg) groups, two-tailed distribution, two-sample unequal variance (heteroscedastic). Fold change for each candidate is indicated.

Additional file 2 - Gene candidates of the sprouting transcriptome (Additional file 2_ColSpr Candidates.xlsx).

List of gene candidates obtained after t-test between triplicates of control and sprouting (ColSpr) groups, two-tailed distribution, two-sample unequal variance (heteroscedastic). Fold change for each candidate is indicated.

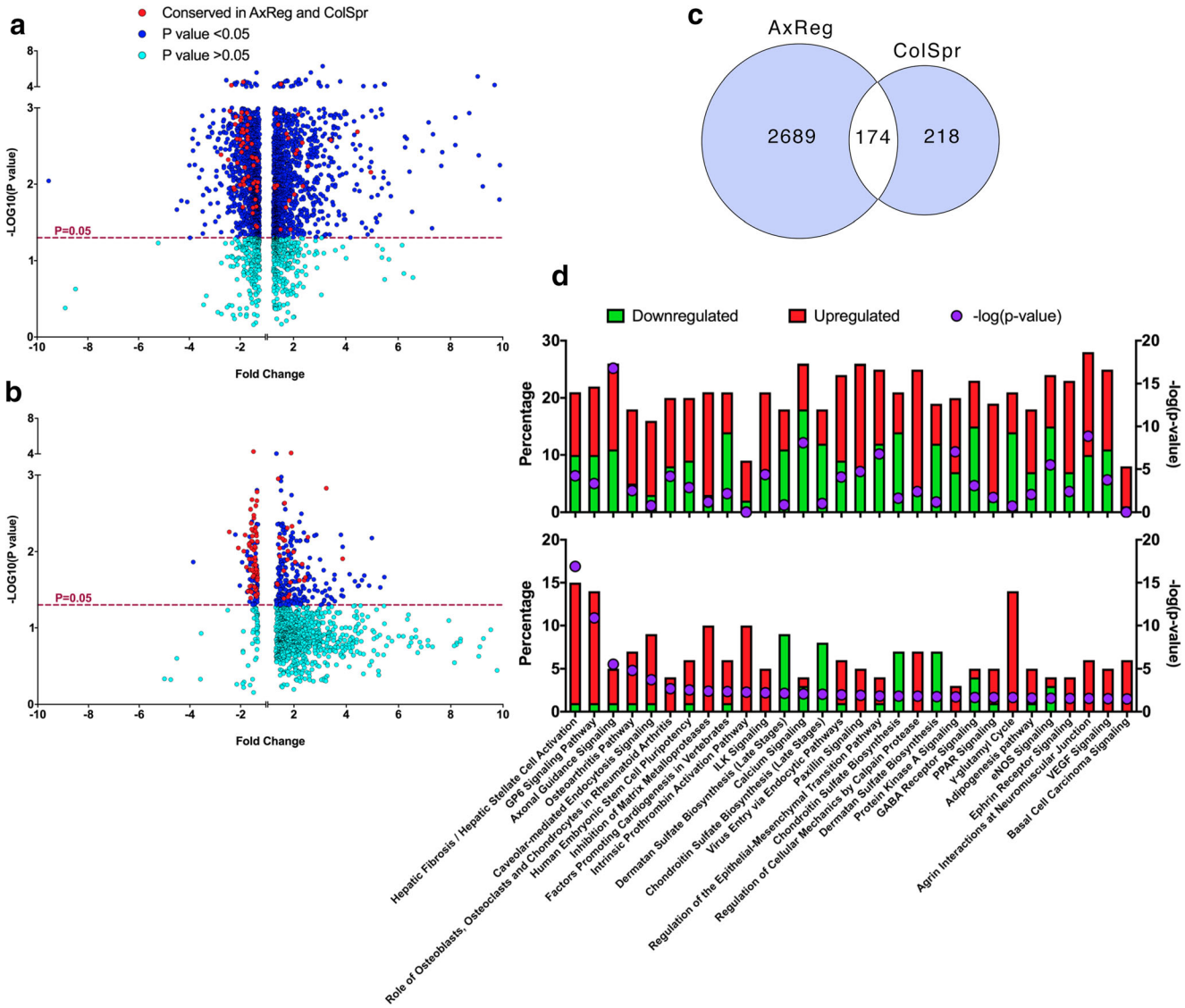

Fig. 5 Transcriptome analysis of L4 DRG neurons conditioned by Wallerian degeneration. (a, b) Volcano plots showing the *p* value versus fold change of differentially expressed genes of axonal regeneration (AxReg) and collateral sprouting (ColSpr) transcriptomes. (c) Venn diagram with the number of differentially expressed and common genes. (d) Top canonical pathways significantly regulated in ColSpr transcriptome (lower graph) and their regulation in AxReg (upper graph). The *x*-axis shows the percentage of transcripts that are regulated (bars) and the −log10 (*p* value) of the pathway (purple circles). In the bars, red indicates upregulation and green downregulation of the pathway

Validation of Gene Candidates and Its Effects on the Intrinsic Growth Capacity of DRG Neurons

To validate transcriptomic analysis, common and differentially expressed genes (DEGs) of the regeneration and sprouting transcriptomes were quantified by quantitative real-time PCR 3 days after sham surgery (control), sciatic nerve crush (AxReg), and L3 SN injury (ColSpr). Serpine1 and Vgf were significantly upregulated in both transcriptomes, while Chrna6, Caly, and Tceal6 mRNA levels were downregulated compared with control (Supplementary Fig. 4, first column). Regeneration-associated DEG included Atf3, Fgf3, Gal, Sprr1a, and Cckbr, all of which showed a significant increase in their mRNA levels in the AxReg condition compared with control and ColSpr (Supplementary Fig. 4, second column). Atf3, Gal, and Sprr1A are known and previously validated RAGs [11, 12]. For validation of the sprouting transcriptome, Gdf10, Acta2, Arhgef5, Mdfi, and Ctgf were analyzed, showing a significant increase in their mRNA levels exclusively in the ColSpr condition compared with control and AxReg (Supplementary Fig. 4, third column).

To evaluate a functional role of candidate genes from the sprouting and regeneration transcriptomes in the PNS, we genetically manipulated L4 DRG neurons and analyzed their intrinsic growth capacity in vitro by Sholl analysis. Candidate gene plasmids with GFP reporter gene or GFP alone as control were electroporated to enhance their expression in cultured adult DRG neurons. Overexpression of the RAGs Atf3 and

Fgf3 resulted in a significant increase in neurite length, as shown by the higher values for maximum radius compared with control neurons (Fig. 6a, b). Neurite branching showed significant differences for both RAGs when the number of branching points was analyzed based on the distance from soma (Fig. 6c); however, the sum of branching points along the neurites showed significant differences only for Fgf3 (Fig. 6d). The enhanced expression of SAGs Gdf10, Arhgef5, and Acta2 significantly increased neurite length compared with control neurons, at similar levels as RAGs Atf3, and Fgf3 (Fig. 6a–c). In addition, overexpression of all SAGs induced a significant increase in neurite branching (Fig. 6d, e), as a characteristic growth process of collateral sprouting.

The characterization of this novel genes contributes to the understanding of an axonal repair mechanism and provides possible therapeutic targets to promote functional recovery after a peripheral nerve injury.

Discussion

Collateral sprouting is an axonal growth response from spared neurons after a nervous system injury, with successful applications on peripheral nerve repair. Unlike axonal regeneration, the molecular mechanisms associated to collateral sprouting have not been fully characterized in the PNS. Here, we developed a novel model to study the process of collateral sprouting and determine that sensory neurons exposed to a Wallerian degeneration environment activate a sprouting-associated transcriptome with unique genes and pathways that increase the intrinsic growth capacity of neurons.

A Novel Collateral Sprouting Model in the PNS

In the model of L3 SN transection, direct interaction between intact axons and degenerated axonal fibers is achieved inside the sciatic nerve. This model offers advantages over other described in vivo models, such as end-to-side nerve repair, in which the perineurium of the donor nerve acts as a barrier for the diffusion of signals from the degenerated environment [38–40]. Moreover, due to the anatomical structure of the sciatic nerve in mice, which is formed by spinal nerves L3, L4, and L5, the model of L3 SN injury allows an easy and practical localization of neuronal somas in which their axons have been spared or damaged, facilitating the characterization of the molecular changes associated to regenerative mechanisms. A new model of end-to-side neurorrhaphy in which the distal end of the transected musculocutaneous nerve is sutured to the median nerve lateral head, allowing direct contact of the degenerated milieu and uninjured axons, was validated and published [7]. In this model, the use of two nerves with different spinal nerve contribution makes the localization and isolation of the sprouting neuronal somas in the DRG difficult, and therefore, the study of collateral sprouting molecular mechanisms. However, our findings agree with the results of Bao et al. (2016) in that the Wallerian degeneration–induced environment is sufficient to induce collateral sprouting of uninjured sensory neurons.

Two weeks after L3 spinal nerve injury, intact L4 SN axons collaterally sprouted into degenerated nerve areas. It is well documented that during collateral sprouting, new sprouts are attracted to the degenerated environment. Decades ago, Diaz and Pecot-dechavassine (1990) revealed that in a degenerated nerve segment placed over a fully functional muscle, diffusible factors released by Schwann cells not only induced sprouting and proliferation of axonal processes, but also drew/attracted collateral axons into the degenerated nerve shaft [15]. This Wallerian degeneration–induced attraction of axonal sprouts has also been shown in models of skin denervation [41–43] and end-to-side neurorrhaphy [7, 38, 44], with successful target reinnervation.

L4 SN collateral axon growth was delayed in our model compared with reported data of growing regenerating axons. Navarro et al. (2007) reviewed that axonal regeneration reaches a constant growth rate of about 2–3 mm/day by 3–4 days after injury [45], much earlier than observed here for collateral sprouting. However, a comparison between end-to-end repair, in which the stumps of the injured nerve are reconnected promoting axonal regeneration, and end-to-side repair, revealed that differences in axonal growth rate and axonal thickness were observed at 6 weeks, which agrees with our results. However, no differences were detected at 12 weeks [2]. Moreover, earlier observations showed that intact axons needed a 2-month delay to collaterally sprout into the recipient nerve in a model of end-to-side compared with end-to-end repair [46]. The hypomyelination of L4 SN collateral sprouts observed 21 days after injury also agrees with the findings of Liao et al. (2009), who showed fewer, thinly myelinated small-diameter motor axons 2 months after end-to-side anastomosis [46]. Nevertheless, g-ratio 40 days after L3 SN injury was found to be lower and still presented a variable axonal size distribution in collateral sprouts compared to uninjured axons. It has been shown that Schwann cells can sense neuronal activity to provide feedback and modulate axonal functions, such as myelination, in an activity-dependent manner [47, 48]. Target innervation of L4 SN collaterals was not assessed in this work and lack of target synapsing could influence the myelination process resulting in hypermyelination. It is also possible that although Schwann cells are myelinating collateral sprouts, they could be reading molecular signals for myelin thickness from the intact sprouting axon, which is probably a large caliber axon.

These results revealed that L3 SN degeneration triggers collateral sprouting of uninjured L4 SN axons inside the sciatic nerve and that collateral axons are attracted to the degenerated environment, as previously described.

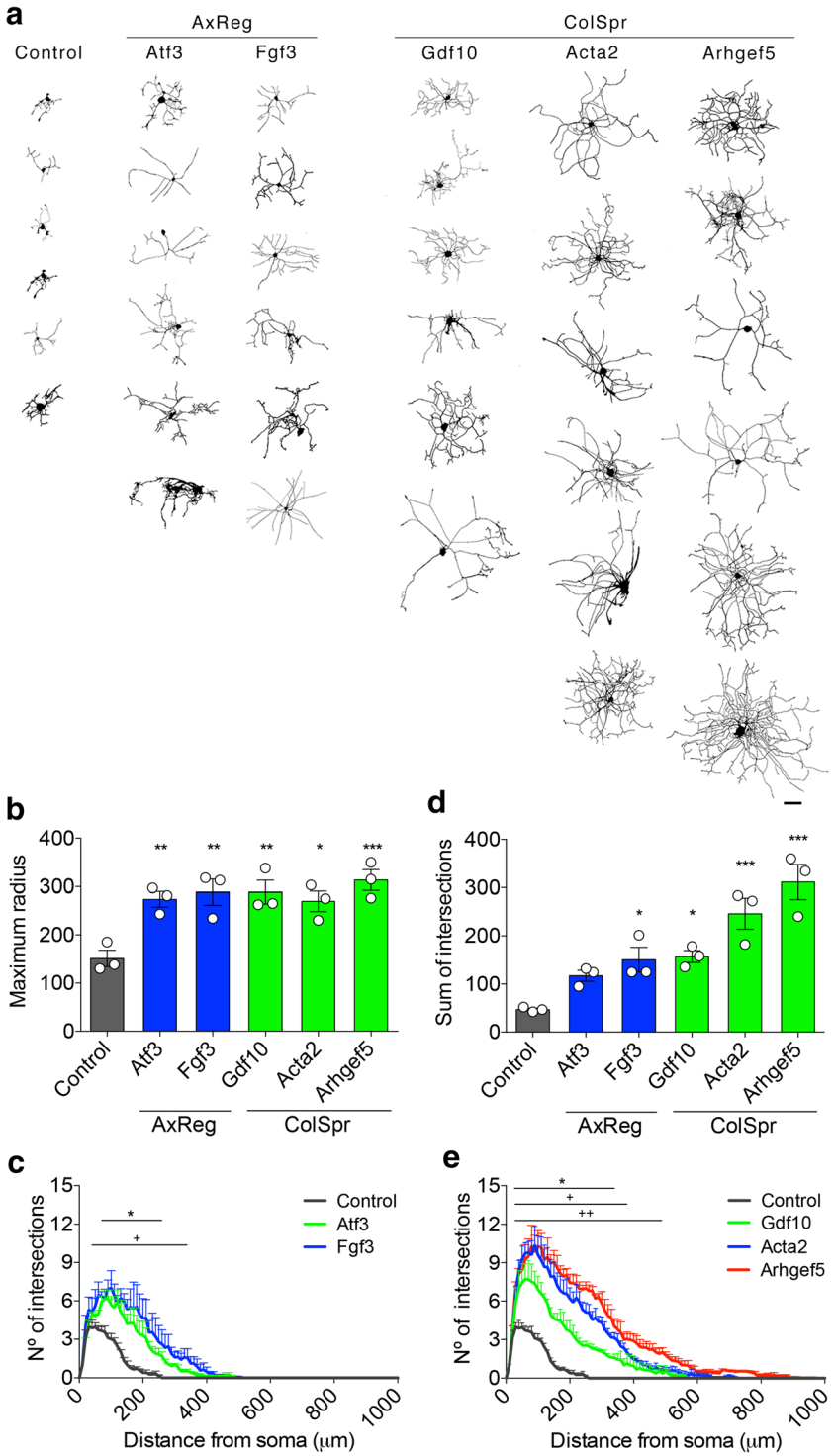

Fig. 6 Manipulation of sprouting-associated genes increase the intrinsic growth of DRG neurons. L4 DRG neurons were electroporated with plasmid expressing regeneration- and sprouting-associated genes and cultured for 48 h; the plasmids also express eGFP to identify electroporated neurons. **a** Images of electroporated L4 DRG neurons identified by GFP (in gray scale) after 48 h in vitro. The 6 largest neurons are shown for each condition. Scale bar 100 μm. **b–e** Neurite outgrowth of electroporated L4 DRG neurons. Concentric circles of 10-μm radius were overlapped on neuron masks around the soma until 1000 μm of distance. The maximum radius reached by neurites was determined after 48 h in vitro (**b**). The number of intersections with concentric circles was quantified after 48 h in vitro and the total sum of intersections (**c**) and the number of intersections versus the distance of concentric circles from soma (**d**, **e**) were plotted. Data is shown as mean ± S.E.M. Comparisons were made between control and each group. In **b** and **c**, statistical significance was determined by one-way ANOVA followed by Bonferroni's post hoc test (*$p < 0.01$, **$p < 0.001$, ***$p < 0.0001$). In **d** and **e**, statistical significance was analyzed by two-way ANOVA followed by Bonferroni's post hoc test. (*$p < 0.05$ for comparisons between control and Atf3 or Gdf10; $^{+}p < 0.05$ for comparisons between control and Fgf3 or Acta2; $^{++}p < 0.05$ for comparisons between control and Arhgef5)

Moreover, collateral sprouts of sciatic nerve axons grew and myelinated in a slower fashion than reported for regenerating fibers.

Molecular Mechanisms of Collateral Sprouting

After nerve damage, injury-related signals activate a regeneration-associated transcriptional program that increases the intrinsic growth capacity of injured neurons [11, 12, 14]. This is clearly demonstrated in the conditioning lesion paradigm, in which a prior conditioning peripheral nerve lesion in vivo promotes earlier neurite outgrowth and more elongated neurites in vitro in DRG neurons because of the orchestrated activation of growth transcriptional profile [34, 49, 50]. We showed that sensory neurons conditioned by a Wallerian degeneration–induced environment increase their intrinsic growth capacity compared to unconditioned neurons. This growth facility was more associated with an increase in neurite branching rather than neurite elongation. On the other hand, DRG neurons conditioned by a direct peripheral nerve injury showed a sustained increase in both parameters. These results show that the axonal growth response triggered after injury and after exposure to a degenerated environment involves different morphological changes and suggests that distinctive molecular mechanisms may underlie both processes. Previously, it was shown that the conditioning lesion effect induced by a prior nerve injury was a combination of different processes, such as neurite initiation, extension, and branching, which vary depending on the nature of the lesion (crush, ligation, or transection) and duration of the culture period [33]. During development, axons sprout to establish networks of neuronal connectivity [51], showing the importance of axonal branching in addition to axonal elongation. Moreover, a dissociation of both mechanisms, as de novo formation of an axon branch from the main axon shaft independent of the growth cone, and the extension of the main axon have been demonstrated, indicating that the mechanisms are not fully conserved [51–53]. This dissociation might explain why after 48 h in culture, degeneration-conditioned DRG neurons exhibit a significant increase in axonal branching compared to unconditioned neurons but not in neurite length, suggesting that Wallerian degeneration activates a specific mechanism dedicated to stimulate collateral sprouting of intact axons, recapitulating axonal branching during development. These findings revealed that the exposure to a degenerated environment increases the intrinsic growth capacity of neurons, but with different morphological changes than the observed after a direct axonal injury. Therefore, it is highly likely that collateral sprouting and axonal regeneration depend on the activation of different transcriptional programs.

Here we demonstrate that the increase in sensory neuronal growth capacity after exposure to the Wallerian degeneration environment is associated with the activation of a particular transcriptional profile, with unique genes that could define the mechanism of collateral sprouting in the PNS as a nerve repair process that is dissociated from canonical axonal regeneration. The number of genes regulated in the collateral sprouting transcriptome was significantly lower than the observed for axonal regeneration. After nerve damage, injury-related signals, such as the interruption of trophic factors transport, retrograde transport of lesion-modified molecules, and increased action potentials discharge from the injury site, induce major changes at the transcriptomic level in the DRG in order to regenerate a whole axon [13, 54]. Collateral sprouting neurons are uninjured cells receiving indirect signals from the axonal degenerated microenvironment, mainly diffusible factors from Schwann cells, which could explain the lower transcriptional response compared to regenerating neurons. Injured neurons besides experiencing changes in their growth status also must react against profound disturbances in metabolism, cell death and survival, neurotransmission, excitability, and inflammation [45, 55, 56], involving the activation of additional signaling pathways. Moreover, L3 SN has a lower contribution of axons to the sciatic nerve than L4 SN, which implies that only a subset of intact neurons is in direct contact with degenerating axons after L3 SN injury, as seen in Fig. 1 c, diluting transcriptional changes associated to axonal sprouting. This hypothesis could be tested by injuring L4 SN and leaving intact L3 SN, increasing the source of the sprouting triggers over spared axons.

The considerable number of genes shared between transcriptomes suggests the regulation of overlapping pathway. This is expected since axonal regeneration and collateral sprouting, although activated by different signals, correspond to axonal growth processes. However, the change in magnitude of these common genes was higher in axonal regeneration than in collateral sprouting, which could be associated with the type of stimulus involved in each axonal growth reaction and the dilution effect of our model, as mentioned above. After analysis of exclusively expressed genes, we observed different regulation tendencies in both transcriptomes. For collateral sprouting, although changes in transcripts were smaller in magnitude, most were upregulated, while in axonal regeneration there was a balance between up- and downregulation, strongly suggesting distinctive molecular mechanisms for both processes. This could be due to the fact that sprouting neurons are responding to a permissive environment rather than directly reacting to an injury process. In agreement with this, the top five canonical pathways differentially regulated in the collateral sprouting transcriptome, excluding Axonal Guidance Signaling, showed very low activation in axonal regeneration, evidencing differentiated regulation of metabolic routes. IPA analysis of the collateral sprouting transcriptional profile revealed the activation of a specific network with upregulation of genes previously involved in axonal sprouting after a CNS injury. In 2010, Li et al. described the

transcriptome associated to the sprouting of peri-infarct cortical neurons after stroke, as a plasticity response of CNS neurons [19]. Later, they showed that signaling through GDF10, which is induced by peri-infarct neurons, activates a unique transcriptional profile different than the activated by developing neurons [20]. Interestingly, we found that Gdf10 and the downstream transcription factors Smad2/3 were upregulated in a highly activated network in the collateral sprouting transcriptome, associated with other significantly regulated novel transcripts, Arhgef5 and Acta2. Guanine nucleotide exchange factors (GEFs) have an important role in the activation and function of small GTPases [57]. The Rho GEF 5, encoded by the gene Arhgef5, have been implicated in cell adhesion, cell migration, and cancer [58, 59]. α-smooth muscle actin, encoded by the gene Acta2, is present in vascular smooth muscle cells with a role in vascular contractile function, and mutations in Acta2 have been associated with the development of vasculopathies [60]. However, these transcripts have not been described in axonal growth processes until now. Functional analysis revealed here that overexpression of SAGs Gdf10, Arhgef5, and Acta2 increased the branching capacity of DRG neurons in a stronger fashion than other recognized RAG, as is Atf3 [50, 61]. Moreover, these novel SAGs were able to enhance neurite elongation at the same level of Atf3. These results suggest that activation of RAGs is triggering growing process mainly directed to axonal elongation of regenerating fibers, while SAGs are not only promoting lineal growth, but also stimulating ramification of axons, as it happens in neurons during development, revealing that axonal regeneration and collateral sprouting are mediated by different molecular mechanisms.

Conclusions

We showed that collateral sprouting from uninjured sensory fibers is associated with the activation of a unique transcriptomic profile, revealing novel sprouting-associated genes (SAGs), not previously associated to axonal regeneration. Identification and validation of these gene candidates provide insights for the generation of new therapeutic tools to promote functional recovery after an injury to the nervous system.

Acknowledgments We thank all the Court Lab members who contributed to this research, especially to Mónica Pérez for her excellent histological processing and Jaime Alvarez for the scientific advice. TMW is supported by ISPG funding from the BBSRC.

Author Contributions DL and FAC planned the project and conducted the experiments. DL performed the L3 and L4 spinal nerve surgeries, processed the samples, and analyzed the histological data. MLH and TW executed the bioinformatic analysis. DL, CDG, MO, and GM contributed with in vitro and molecular analysis. AC and MO contributed with nerve surgeries. DL and FAC wrote the manuscript. All authors read and approved the final manuscript.

Funding Information All the experiments, including collection and analysis of data, was supported by FONDECYT-1150766, FONDECYT-1190518, Geroscience Center for Brain Health and Metabolism FONDAP-15150012 and Millennium Institute No. P09-015-F. A scholarship from the Formation of Advance Human Capital Program of CONICYT (no. 21110017) supported the design of the study, data interpretation, and manuscript writing. Thomas M. Whishart is supported by ISPG funding from the BBSRC.

Data Availability The datasets analyzed in this article are available from the corresponding author on a reasonable request.

Compliance with Ethical Standards

Competing Interests The authors declare that they have no competing interests.

Abbreviations RAGs, regeneration-associated genes; PNS, peripheral nervous system; Wld^S, transgenic mice with delayed Wallerian degeneration; SAGs, sprouting-associated genes; CNS, central nervous system; SCI, spinal cord injury; DRG, dorsal root ganglia; SN, spinal nerve; Dpi, days post-injury; BDA, biotinylated dextran amine; EM, electron microscopy; NFM, neurofilament median chain; ATF3, activating transcription factor 3; NFH, neurofilament heavy chain; MBP, myelin basic protein; p75NTR, p75 neurotrophin receptor; RNA, ribonucleic acid; mRNA, messenger ribonucleic acid; RT-PCR, real-time polymerase chain reaction; RNA-seq, RNA sequencing; GFP, green fluorescent protein; Fgf3, fibroblast growth factor 3; Gdf10, growth differentiation factor 10; Acta2, actin alpha 2; Arhgef5, rho guanine nucleotide exchange factor 5; IPA, Ingenuity Pathway Analysis; DEG, differentially expressed genes

References

1. Panagopoulos GN, Megaloikonomos PD, Mavrogenis AF (2017) The present and future for peripheral nerve regeneration. Orthopedics. 40(1):e141–e156
2. Tateshita T, Ueda K, Kajikawa A (2018) End-to-end and end-to-side neurorrhaphy between thick donor nerves and thin recipient nerves : an axon regeneration study in a rat model. Neural Regen Res 13(4):699–703
3. Ray WZ, Mackinnon SE (2010) Management of nerve gaps : autografts, allografts, nerve transfers, and end-to-side neurorrhaphy. Exp Neurol 223(1):77–85
4. Carmichael ST, Chesselet M-F (2002) Synchronous neuronal activity is a signal for axonal sprouting after cortical lesions in the adult. J Neurosci 22(14):6062–6070
5. Bareyre FM, Kerschensteiner M, Raineteau O, Mettenleiter TC, Weinmann O, Schwab ME (2004) The injured spinal cord spontaneously forms a new intraspinal circuit in adult rats. Nat Neurosci 7(3):269–277
6. Collyer E, Catenaccio A, Lemaitre D, Diaz P, Valenzuela V, Bronfman F, Court FA (2014) Sprouting of axonal collaterals after spinal cord injury is prevented by delayed axonal degeneration. Exp Neurol 261:451–461
7. Bao Q, Xiao C, Wang T, Gu Y (2016) Novel atraumatic end-to-side repair model exhibits robust collateral sprouting independent of donor fiber injury. Plast Reconstr Surg 137(2):523–533
8. Civi S, Durdag E, Aytar MH, Kardes O, Kaymaz F, Aykol S (2017) Usefulness of end-to-side bridging anastomosis of sural nerve to

tibial nerve : an experimental research. J Korean Neurosurg Soc 60(4):417–423
9. Ballance CA, Ballance HA, Stewart P (1903) Remarks on the operative treatment of chronic facial palsy of peripheral origin. Br Med J 1(2209):1009–1013
10. Viterbo F, Trindade J, Hoshino K, Mazzoni NA (1992) Latero-terminal neurorrhaphy without removal of the epineural sheath. Experimental study in rats. Rev Paul Med 110(6):267–275
11. Ma TC, Willis DE (2015) What makes a RAG regeneration associated? Front Mol Neurosci [Internet] 8(43):1–13. Available from:. https://doi.org/10.3389/fnmol.2015.00043/abstract
12. Chandran V, Coppola G, Nawabi H, Omura T, Versano R, Huebner EA, Zhang A, Costigan M et al (2016) A systems-level analysis of the peripheral nerve intrinsic axonal growth program. Neuron [Internet] 89(5):956–970. Available from:. https://doi.org/10.1016/j.neuron.2016.01.034
13. Perlson E, Hanz S, Medzihradszky KF, Burlingame AL, Fainzilber M (2004) From snails to sciatic nerve: retrograde injury signaling from axon to soma in lesioned neurons. J Neurobiol 58(2):287–294
14. Michaelevski I, Segal-ruder Y, Rozenbaum M, Medzihradszky KF, Shalem O, Coppola G et al (2010) Signaling to transcription networks in th neuronal retrograde injury response. Sci Signal 3(130): ra53
15. Diaz BYJ, Pecot-dechavassine M (1990) Nerve sprouting induced by a piece of peripheral nerve placed over a normally innervated frog muscle. J Physiol 421:123–133
16. Dubový P, Raška O, Klusáková I, Stejskal L, Čelakovský P, Haninec P (2011) Ciliary neurotrophic factor promotes motor reinnervation of the musculocutaneous nerve in an experimental model of end-to-side neurorrhaphy. BMC Neurosci 12:58
17. Bosse F (2012) Extrinsic cellular and molecular mediators of peripheral axonal regeneration. Cell Tissue Res 349(1):5–14
18. Wang JT, Medress ZA, Barres BA (2012) Axon degeneration: molecular mechanisms of a self-destruction pathway. J Cell Biol 196(1):7–18
19. Li S, Overman JJ, Katsman D, Kozlov SV, Donnelly CJ, Twiss JL et al (2010) An age-related sprouting transcriptome provides molecular control of axonal sprouting after stroke. Nat Publ Gr [Internet] 13(12):1496–1504. Available from:. https://doi.org/10.1038/nn.2674
20. Li S, Nie EH, Yin Y, Benowitz LI, Tung S, Vinters HV et al (2015. Available from:) GDF10 is a signal for axonal sprouting and functional recovery after stroke. Nat Neurosci [Internet]. https://doi.org/10.1038/nn.4146
21. Weidner N, Ner A, Salimi N, Tuszynski MH (2001) Spontaneous corticospinal axonal plasticity and functional recovery after adult central nervous system injury. Proc Natl Acad Sci U S A 98(6): 3513–3518
22. Fink KL, López-Giráldez F, Strittmatter SM, Cafferty WBJ (2017) Identification of intrinsic axon growth modulators for intact CNS neurons after injury. Cell Rep 18(11):2687–2701
23. Yang P, Yang Z (2012) Enhancing intrinsic growth capacity promotes adult CNS regeneration. J Neurol Sci [Internet] 312(1–2):1–6. Available from:. https://doi.org/10.1016/j.jns.2011.08.037
24. O'Donovan KJ (2016) Intrinsic axonal growth and the drive for regeneration. Front Neurosci 10(486):1–11
25. Richardson PM, Issa V (1984) Peripheral injury enhances central regeneration of primary sensory neurones. Nature. 309(5971):791–793
26. Catenaccio A, Llavero Hurtado M, Diaz P, Lamont DJ, Wishart TM, Court FA (2017) Molecular analysis of axonal-intrinsic and glial-associated co-regulation of axon degeneration. Cell Death Dis [Internet] 8(11):1–14. Available from:. https://doi.org/10.1038/cddis.2017.489
27. Llavero Hurtado M, Fuller HR, Wong AMS, Eaton SL, Gillingwater TH, Pennetta G et al (2017) Proteomic mapping of differentially vulnerable pre-synaptic populations identifies regulators of neuronal stability in vivo. Sci Rep 7(1):1–18
28. Rigaud M, Gemes G, Barabas ME, Chernoff DI, Abram SE, Stucky CL, Hogan QH (2008) Species and strain differences in rodent sciatic nerve anatomy: Implications for studies of neuropathic pain. Pain. 136(1–2):188–201
29. Hirata K, Kawabuchi M (2002) Myelin phagocytosis by macrophages and nonmacrophages during Wallerian degeneration. Microsc Res Tech 57(6):541–547
30. Barrientos SA, Martinez NW, Yoo S, Jara JS, Zamorano S, Hetz C, Twiss JL, Alvarez J et al (2011) Axonal degeneration is mediated by the mitochondrial permeability transition pore. J Neurosci 31(3): 966–978
31. Fex Svennigsen Å, Dahlin LB (2013) Repair of the peripheral nerve—remyelination that works. Brain Sci 3(3):1182–1197
32. Oñate M, Catenaccio A, Martínez G, Armentano D, Parsons G, Kerr B, Hetz C, Court FA (2016) Activation of the unfolded protein response promotes axonal regeneration after peripheral nerve injury. Nat Publ Gr [Internet] 6(21709):1–14. Available from:. https://doi.org/10.1038/srep21709
33. Lankford KL, Waxman SG, Kocsis JD, Haven W (1998) Mechanisms of enhancement of neurite regeneration in vitro following a conditioning sciatic nerve lesion. J Comp Neurol 391:11–29
34. Hoffman PN (2010) A conditioning lesion induces changes in gene expression and axonal transport that enhance regeneration by increasing the intrinsic growth state of axons. Exp Neurol [Internet]. 223(1):11–18. Available from:. https://doi.org/10.1016/j.expneurol.2009.09.006
35. Madison RD, Zomorodi A, Robinson GA (2000) Netrin-1 and peripheral nerve regeneration in the adult rat. Exp Neurol 161(2):563–570
36. Parrinello S, Napoli I, Ribeiro S, Digby PW, Fedorova M, Parkinson DB, Doddrell RDS, Nakayama M et al (2010) EphB signaling directs peripheral nerve regeneration through Sox2-dependent Schwann cell sorting. Cell [Internet] 143(1):145–155. Available from:. https://doi.org/10.1016/j.cell.2010.08.039
37. Dun X, Parkinson DB (2017) Role of Netrin-1 Signaling in Nerve Regeneration. Int J Mol Sci 18(3):491.
38. Haninec P, Kaiser R, Dubový P (2012) A comparison of collateral sprouting of sensory and motor axons after end-to-side neurorrhaphy with and without the perineurial window. Plast Reconstr Surg 130(3):609–614
39. Liu H, Chen Z-G, Lineaweaver WC, Zhang F (2016) Can the babysitter procedure improve nerve regeneration and denervated muscle atrophy in the treatment of peripheral nerve injury? Plast Reconstr Surg 138(1):122–131
40. Liu P, Liao C, Zhong W, Yang M, Li P, Zhang W (2018) Comparison of 4 different methods for direct hypoglossal-facial nerve anastomosis in rats. World Neurosurg [Internet] 112:e588–e596. Available from:. https://doi.org/10.1016/j.wneu.2018.01.094
41. Kinnman E, Aldskogius H (1986) Collateral sprouting of sensory axons in the glabrous skin of the hindpaw after chronic sciatic nerve lesion in adult and neonatal rats: a morphological study. Brain Res 377(1):73–82
42. Diamond J, Holmes M, Coughlin M (1992) Endogenous NGF and nerve impulses regulate the collateral sprouting of sensory axons in the skin of the adult rat. J Neurosci 12(4):1454–1466
43. Cobianchi S, de Cruz J, Navarro X (2014) Assessment of sensory thresholds and nociceptive fiber growth after sciatic nerve injury reveals the differential contribution of collateral reinnervation and nerve regeneration to neuropathic pain. Exp Neurol [Internet] 255: 1–11. Available from:. https://doi.org/10.1016/j.expneurol.2014.02.008
44. Lundborg G, Zhao Q, Kanje M, Danielsen N, Kerns J (1994) Can sensory and motor collateral sprouting be induced from intact

peripheral nerve by end-to-side anastomosis? J Hand Surg Br 19(3): 277–282
45. Navarro X, Vivó M, Valero-Cabré A (2007) Neural plasticity after peripheral nerve injury and regeneration. Prog Neurobiol 82(4): 163–201
46. Liao W, Chen J, Wang Y, Tseng G (2009) The efficacy of end-to-end and end-to-side nerve repair (neurorrhaphy) in the rat brachial plexus. J Anat 215:506–521
47. Stevens B, Tanner S, Fields RD (1998) Control of myelination by specific patterns of neural impulses. J Neurosci 18(22):9303–9311
48. Samara C, Poirot O, Domènech-estévez E, Chrast R (2013) Neuronal activity in the hub of extrasynaptic Schwann cell-axon interactions Edited by : Reviewed by. Front Cell Nuerosci 7(228): 1–11
49. Knott EP, Assi M, Pearse DD (2014) Cyclic AMP signaling : a molecular determinant of peripheral nerve regeneration. Biomed Res Int 2014(651625):1–8
50. Fagoe ND, Attwell CL, Kouwenhoven D, Verhaagen J, Mason MRJ (2015) Overexpression of ATF3 or the combination of ATF3 , c-Jun , STAT3 and Smad1 promotes regeneration of the central axon branch of sensory neurons but without synergistic effects. Hum Mol Genet 24(23):6788–6800
51. Gallo G (2011) The cytoskeletal and signaling mechanisms of axon collateral branching. Dev Neurobiol 71(3):201–220
52. Dent EW, Kalil K (2001) Axon branching requires interactions between dynamic microtubules and actin filaments. J Neurosci 21(24):9757–9769
53. Bouquet C, Soares S, von Boxberg Y, Ravaille-Veron M, Propst F, Nothias F (2004) Microtubule-associated protein 1B controls directionality of growth cone migration and axonal branching in regeneration of adult dorsal root ganglia neurons. J Neurosci 24(32): 7204–7213
54. Kiryu-Seo S, Kiyama H (2011) The nuclear events guiding successful nerve regeneration. Front Mol Neurosci [Internet] 4(53):1–11. Available from:. https://doi.org/10.3389/fnmol.2011.00053/abstract
55. Costigan M, Befort K, Karchewski L, Griffin RS, D'Urso D, Allchorne A et al (2002) Replicate high-density rat genome oligonucleotide microarrays reveal hundreds of regulated genes in the dorsal root ganglion after peripheral nerve injury. BMC Neurosci 3: 1–18
56. Niemi JP, DeFrancesco-Lisowitz A, Cregg JM, Howarth M, Zigmond RE (2016) Overexpression of the monocyte chemokine CCL2 in dorsal root ganglion neurons causes a conditioning-like increase in neurite outgrowth and does so via a STAT3 dependent mechanism. Exp Neurol [Internet]. 275:25–37. Available from:. https://doi.org/10.1016/j.expneurol.2015.09.018
57. Cherfils J, Zeghouf M (2013) Regulation of small GTPases by GEFs, GAPs, and GDIs. Physiol Rev 93(1):269–309
58. Kuroiwa M, Oneyama C, Nada S, Okada M (2011) The guanine nucleotide exchange factor Arhgef5 plays crucial roles in Src-induced podosome formation. J Cell Sci 124:1726–1738
59. Huang O, Wu D, Xie F, Lin L, Wang X, Jiang M, Li Y, Chen W et al (2015) Targeting rho guanine nucleotide exchange factor ARHGEF5 / TIM with auto-inhibitory peptides in human breast cancer. Amino Acids [Internet] 47(6):1239–1246. Available from: . https://doi.org/10.1007/s00726-015-1950-0
60. Yuan S (2015) α-Smooth muscle actin and ACTA2 gene expressions in vasculopathies. Brazilian J Cardiovasc Surg 30(6):644–649
61. Seijffers R, Mills CD, Woolf CJ (2007) ATF3 increases the intrinsic growth state of DRG neurons to enhance peripheral nerve regeneration. J Neurosci [Internet] 27(30):7911–7920. Available from:. https://doi.org/10.1523/JNEUROSCI.5313-06.2007